CESifo WORKING PAPERS

9475
2021

December 2021

# How Do Pandemics End? Two Decades of Recurrent Outbreak Risk Following the Main Waves

*Max Schroeder, Spyridon Lazarakis, Rebecca Mancy, Konstantinos Angelopoulos*

CESifo

## Impressum:

CESifo Working Papers
ISSN 2364-1428 (electronic version)
Publisher and distributor: Munich Society for the Promotion of Economic Research - CESifo GmbH
The international platform of Ludwigs-Maximilians University's Center for Economic Studies and the ifo Institute
Poschingerstr. 5, 81679 Munich, Germany
Telephone +49 (0)89 2180-2740, Telefax +49 (0)89 2180-17845, email office@cesifo.de
Editor: Clemens Fuest
https://www.cesifo.org/en/wp
An electronic version of the paper may be downloaded
· from the SSRN website: www.SSRN.com
· from the RePEc website: www.RePEc.org
· from the CESifo website: https://www.cesifo.org/en/wp

CESifo *Working Paper No. 9475*

# How do Pandemics End? Two Decades of Recurrent Outbreak Risk Following the Main Waves

## Abstract

The risk of recurrent outbreaks following the main waves of a pandemic has been acknowledged. We provide evidence of the scale and duration of this outbreak risk. We compile municipal public health records and use national data to model the stochastic process of mortality rates after the main pandemic waves of two historical pandemics across multiple locations. For the 1890-91 influenza pandemic in England and Wales, as well as the 1918-19 influenza pandemic in the US and eight major UK cities, we find elevated mortality risk that persists for nearly two decades. The generality of the findings suggests that, without modern means of intervention, post-pandemic outbreak risk is likely to persist for an extended period, as we demonstrate in an application to COVID-19.

Keywords: pandemics, outbreak risk, influenza, Covid-19, archive data.

*Max Schroeder*
*University of Glasgow / United Kingdom*
*max.schroder@glasgow.ac.uk*

*Spyridon Lazarakis*
*Lancaster University / United Kingdom*
*s.lazarakis@lancaster.ac.uk*

*Rebecca Mancy*
*University of Glasgow / United Kingdom*
*rebecca.mancy@glasgow.ac.uk*

*Konstantinos Angelopoulos*
*University of Glasgow / United Kingdom*
*rebecca.mancy@glasgow.ac.uk*

## Introduction

Pandemics are large negative system-wide shocks, increasing health and income risk and affecting humans via reductions in income and wellbeing (e.g. Madhav *et al.*, (2017), Scheidel (2018), Marmot (2020), Marmot and Allen (2020) and Stantcheva (2021)). However, pandemics are not one-off events. Following the main waves of a pandemic, the risk of recurrent outbreaks may remain high due to re-introductions of the virus, new variants, waning immunity, human behaviour (e.g. vaccine refusal), or population turnover that reduces population-level immunity (e.g. Anderson and May (1992) and Oxford (2000)). Indeed, researchers have expressed concern about disease outbreak risk following COVID-19 in academic outlets (e.g. Giannitsarou *et al.* (2021), Kissler *et al.* (2020), Lavine *et al.* (2021), Phillips (2021)) and the media (e.g. McKie (2021)).

Given the effect of pandemics on health and socioeconomic outcomes (e.g. Marmot (2020), Marmot and Allen (2020), Angelopoulos *et al.* (2021b), and Mamelund and Dimka (2021)), a characterisation of medium-run mortality risk and the rate at which it fades is essential to respond appropriately in the coming decades. Evidence from a period without recent advances in medicine, public health and technology can uncover the underlying epidemiological risk before the effect of modern means of intervention and thus highlight the importance of such intervention.

## Empirical observations: post-pandemic mortality rates

We use evidence from two important historical pandemics to shed light on the persistence of recurrent outbreak risk following the main waves. We compiled data on historical mortality rates from influenza for eight large municipalities across the UK, for England and Wales combined, and for the US. Specifically, we gathered city-level data on annual influenza mortality rates between 1895 and 1950 from public health records kept at the municipal level in the UK, namely the Medical Officer for Health (MOH) reports (for details see Supplementary Information (SI)), and used published data for England and Wales and the US.

Figure 1 shows the time series of annual mortality rates from influenza for the different geographies. The key insight from the time series in Figure 1(a)-(j) is that mortality rates remain elevated and more variable for a long period after pandemics. Focusing on the eight British municipalities (a)-(h), although the most striking feature is the massive increase in mortality in 1918 and 1919 due to the main pandemic waves, we also observe spikes of high mortality in the series post-1920 that continue for an extended period. Indeed, contemporary expert evaluations by the Medical Officer for London also identify 1922, 1924, 1927, 1929, 1933 and 1937 as years of elevated influenza mortality (see SI). The same pattern emerges for influenza mortality rates in the US (i), and a similar pattern of disease outbreaks is observed in the aftermath of the 1890-91 influenza pandemic in England and Wales (j).

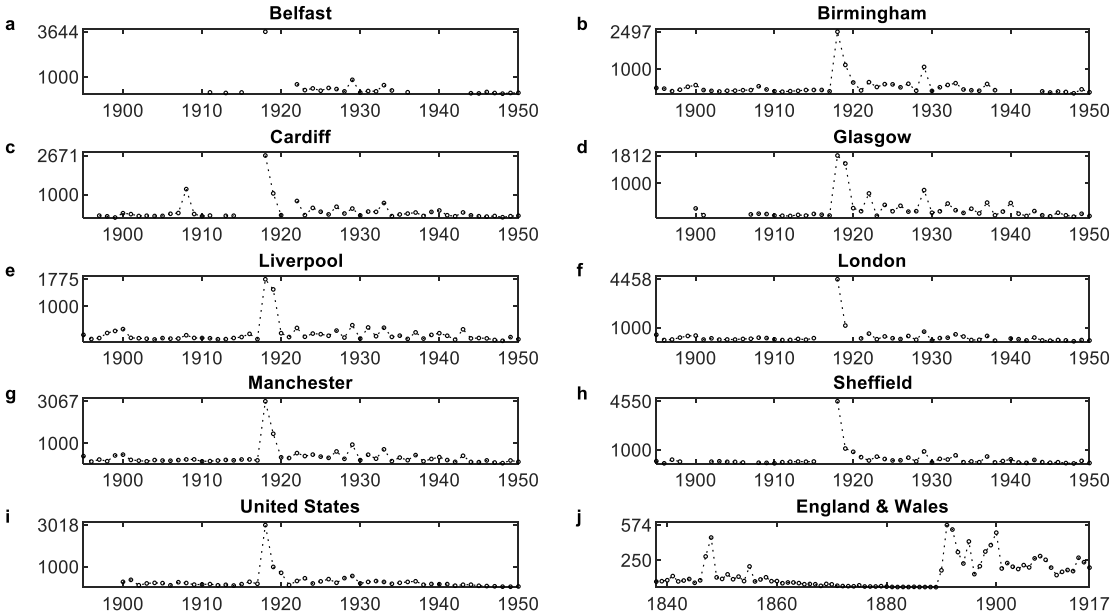


*Figure 1. Annual mortality rate from influenza. Mortality rate in deaths per million population. The upper y-axis tick indicates the maximum mortality rate for each data series. Data for UK cities are taken from Medical Officer for Health reports. Data for the US are taken from Lindner and Grove (1943) and Grove and Hetzel (1968). Data for England & Wales are taken from Langford (2002), Table 5.*

## Model of recurrent outbreak dynamics

To characterise the persistence of disease outbreak risk quantitatively, we conduct formal statistical analysis, modelling the time series of mortality rates following the main waves as outcomes drawn from a sequence of bounded Pareto distributions such that mortality risk and the probability of large outbreaks declines over time. The size of outbreaks has been shown to be highly over-dispersed and is therefore well modelled by a fat-tailed distribution such as a bounded Pareto (e.g. Cirillo and Taleb (2020)). We assume that the inverse of the tail index of the bounded Pareto distributions decays exponentially after the main waves of the pandemic. Denote the mortality rate in year $t$ by $d_t$, for $t = 0,1,2,\dots,N$, where the time period refers to $(1920, 1921, \dots, 1950)$ for the eight cities in the UK and the US with reference the 1918-19 pandemic, and to $(1892, 1893, \dots, 1917)$ for England and Wales with reference to the 1890-91 pandemic.

In each year, mortality rates are drawn from

$$d_t \sim PD_t(d_l, d_u, \alpha_t), \qquad (1)$$

where $PD_t$ denotes the bounded Pareto distribution in period $t$, $\alpha_t > 0$ is the time varying Pareto tail index, and $d_l > 0$ and $d_u > d_l$ are, respectively, lower and upper bounds. Defining $\eta_t = {}^{1}/_{\alpha_t}$, we assume the time process

$$\eta_t = \eta_0 e^{-\lambda t}, \qquad (2)$$

where $\lambda > 0$ determines the rate at which the inverse tail index decays over time, while $\eta_0$ sets the initial level of the probabilities.

We now justify our two main modelling assumptions: firstly, that the mortality rates follow a bounded Pareto distribution; and secondly, that mortality risk declines following the main waves. The bounded Pareto distribution has been used previously in modelling outbreak fatality risk (see Cirillo and Taleb (2020)) and suits our purposes because it offers both flexibility and tractability. A model of the dynamics of mortality risk after the main pandemic waves needs to be sufficiently flexible to capture risk both during the period of relatively high mortality immediately after the main waves and that of lower mortality a few decades later. It is also important that the underlying distribution in any given year can simultaneously capture the potential for large outbreaks via a fat tail, while the mass of the distribution remains at the lower end of mortality. Over time, the tail becomes less important and the distribution converges to a very high concentration toward the lower bound of mortality rates. The bounded Pareto distribution has the flexibility to account for these characteristics: it has a fat tail while the most likely outcomes remain near the lower bound of mortality. Further, it has the advantage of tractability because, conditional on the bounds, a transition in the tail probabilities is identified via changes in one parameter (further discussion on these points, and robustness, can be found in SI).

The decline in mortality risk over time, captured in the model assumption in (1)-(2) is motivated by the empirical observations shown in Figure 1. These observations imply that influenza mortality risk immediately after the main pandemic waves starts from a relatively high level, eventually converging to background mortality (i.e. a level comparable with that immediately prior to the relevant pandemic, as well as several decades later). Under the assumption that risk decreases over time, the model in (1)-(2) describes the level and rate of decline as a function of the parameters $\eta_0$ and $\lambda$, which determine the sequence $(\alpha_t)_{t=0}^{N}$. Although (2) constrains the inverse of the tail index $\alpha_t$ to decay exponentially, it does not impose such a restriction on probabilities associated with the tails. Indeed, although the probabilities of different mortality rates are a monotonic function of the tail index and thus decrease over time, the inverse of a convex function does not have a predetermined convexity, and $\lambda>0$ implies that the rate of decline of the probabilities can take on a range of forms. This feature is evident in the results.

We fit the model to the data after the main pandemic waves, taking as given the main pandemic event. During subsequent recurrent outbreaks, mortality is lower, so we set the upper bound of mortality rates to the maximum mortality rate of the main waves. Similarly, we set the lower bound of mortality to the lowest mortality experienced in the longer run, i.e. background influenza mortality. Our main results are robust to modelling $d_l$ and $d_u$ as theoretical upper and lower bounds of mortality rates (see SI), but by exploiting information pertinent to the pandemic and geographic unit in parameterising $d_l$ and $d_u$, the model provides more accurate mortality risk predictions. Moreover, by letting the bounds differ between geographical units, we allow for differences in the mortality of the main pandemic waves, as well as in latent socioeconomic and public health conditions that can impact mortality associated with these bounds. In turn, this permits applications to predict medium-run mortality risk after the

main waves of other pandemics by conditioning on an upper and lower bound that are relevant for the pandemic and disease in question. We fit the models to the data by choosing the parameters to maximise the likelihood function (see SI for further discussion of modelling choices and for the estimated parameters).

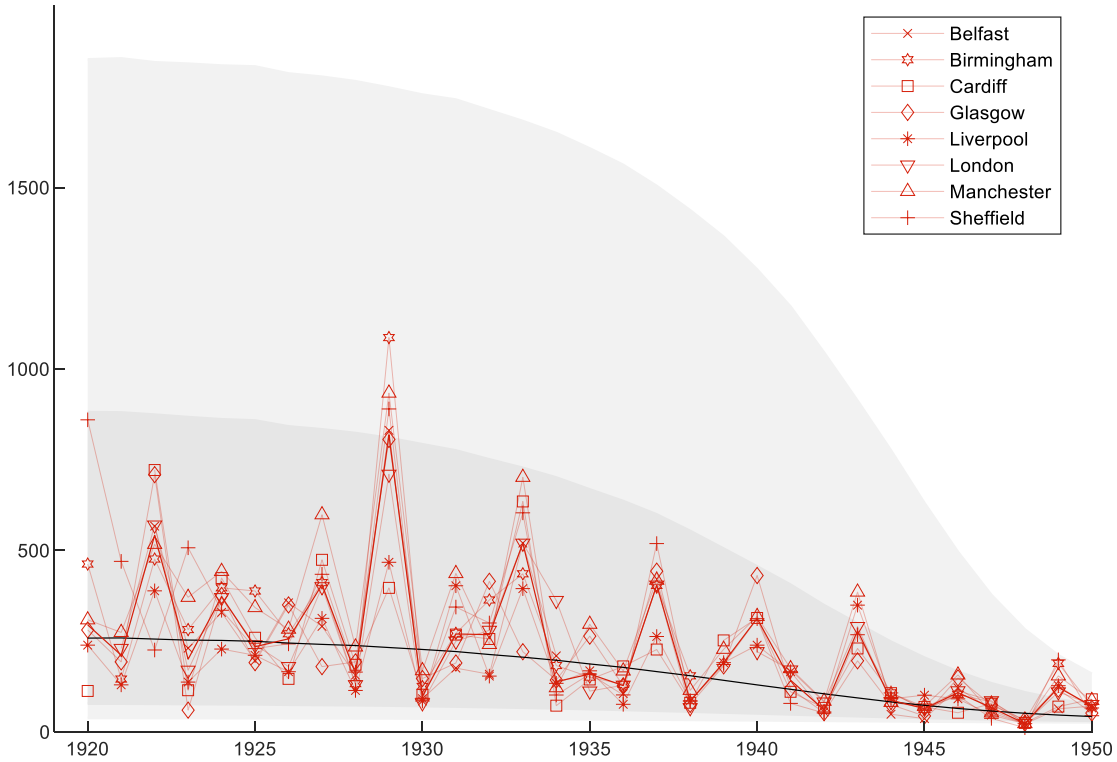


*Figure 2: Simulated median (solid black line), interquartile range (dark shading) and 80% prediction interval (light shading), based on 1m random draws of the model fitted using the average mortality rates across cities, with data overplotted in red.*

Figure 2 shows the time series of data points overlaid on model simulations, defining as the geographical unit, the average rate across the UK cities to set the bounds on the Pareto distributions, and confirm that most observations are contained within the interquartile range of simulated outcomes. Observed outcomes outside these bounds are indeed those of the rarer events: the very large outbreak of 1929 in four cities, and outbreaks in later decades that are less affected by the modelled pandemic. Model predictions for the US, and England and Wales following the 1890-91 pandemic, are consistent with this pattern (see Figure C-1 in SI).

By fitting the models to the data, we obtain the time series of distributions of mortality rates in the decades that follow the main pandemic waves. We can therefore calculate the probability of specified mortality rates by year and compute the time series of disease outbreak risk by defining an outbreak as mortality above a threshold. Figure 3 shows the post-pandemic disease outbreak probabilities for different thresholds, defined taking into account the impact of the main pandemic waves. In particular, for the 1918-19 pandemic, we define two disease outbreak thresholds at 500 and 1000 deaths per million. The 500 per million threshold is about one third of the rate of the main waves (1918 and 1919) and significantly higher than any mortality rate between 1900 and 1918 (i.e. after the 1890-91 pandemic effects had died out). It also corresponds to that

observed during the main waves of the 1890-91 pandemic and subsequent outbreaks. For the period after 1920, this threshold identifies as outbreaks the same years as those described as having exceptionally high mortality in the MOH reports for London. The 1000 per million threshold corresponds to recurrent disease outbreaks approaching the levels experienced in some cities during the main pandemic waves of 1918-19 and approximates that of the severe 1929 outbreak. More generally, this threshold identifies particularly severe disease outbreaks that were *possible* given the dynamic process for mortality risk, even if unrealised *ex post*. Following a similar reasoning, for the 1890-1891 pandemic in England and Wales, we show post-pandemic disease outbreak probabilities for different thresholds that are motivated by mortality during the main pandemic waves and prior to the pandemic.

Figure 3 shows the probabilities of a disease outbreak exceeding different thresholds. Two main results stand out. First, the probability of a disease outbreak remains high for about two decades after the main pandemic waves, and unlike the exponential decline of the tail parameter, declines only very slowly during this period. Second, the pattern of the time evolution is similar across all geographical units, despite considerable differences in the scale of the main waves and in background influenza mortality (Figure 1).

**Application to COVID-19: Lessons from the past for the present**

We use the historical mortality risk estimates to simulate mortality dynamics after the main waves of COVID-19, with the aim of uncovering the underlying epidemiological risk before the effect of modern means of intervention. The generality of the main qualitative characteristics of the dynamic risk patterns in Figure 3, across geographical units with different experience of the main wave and background mortality, suggests that the model in (1) – (2) can be used for counterfactual analysis. Nevertheless, the quantitative predictions are dependent on the bounds of the Pareto distributions, as well as the specific sequence $(\alpha_t)_{t=0}^{N}$ used, or equivalently on the underlying parameter values for $\eta_0$ and $\lambda$. The bounds of the Pareto distributions are determined by the experience of the pandemic to which the model predictions apply. We thus set the upper bound on future mortality to be determined by COVID-19 mortality in the UK in 2020 and the lower bound to reflect mortality in the non-pandemic state in the coming decades, which we approximate by background influenza mortality pre-2020.

Regarding the parameters $\eta_0$ and $\lambda$, inspection of the historical parameters (SI Table B-1) suggests that even though these are relatively similar, there is some variation across geographical units. This generates model uncertainty regarding the risk projections because it creates uncertainty about which sequence of bounded Pareto distributions generates the data. This is a different kind of uncertainty from the epidemiological uncertainty that governs the probability of an outbreak in each year for a given sequence of distributions. To account for uncertainty regarding the dynamic path of disease outbreak risk, given the bounds for the Pareto distributions, we use the range of values of $\eta_0$ and $\lambda$ across the different geographical units from our historical analysis to approximate the

joint distribution of possible parameter values. Then, for one million draws from this joint distribution, we compute the disease outbreak probabilities and compute relevant percentiles.

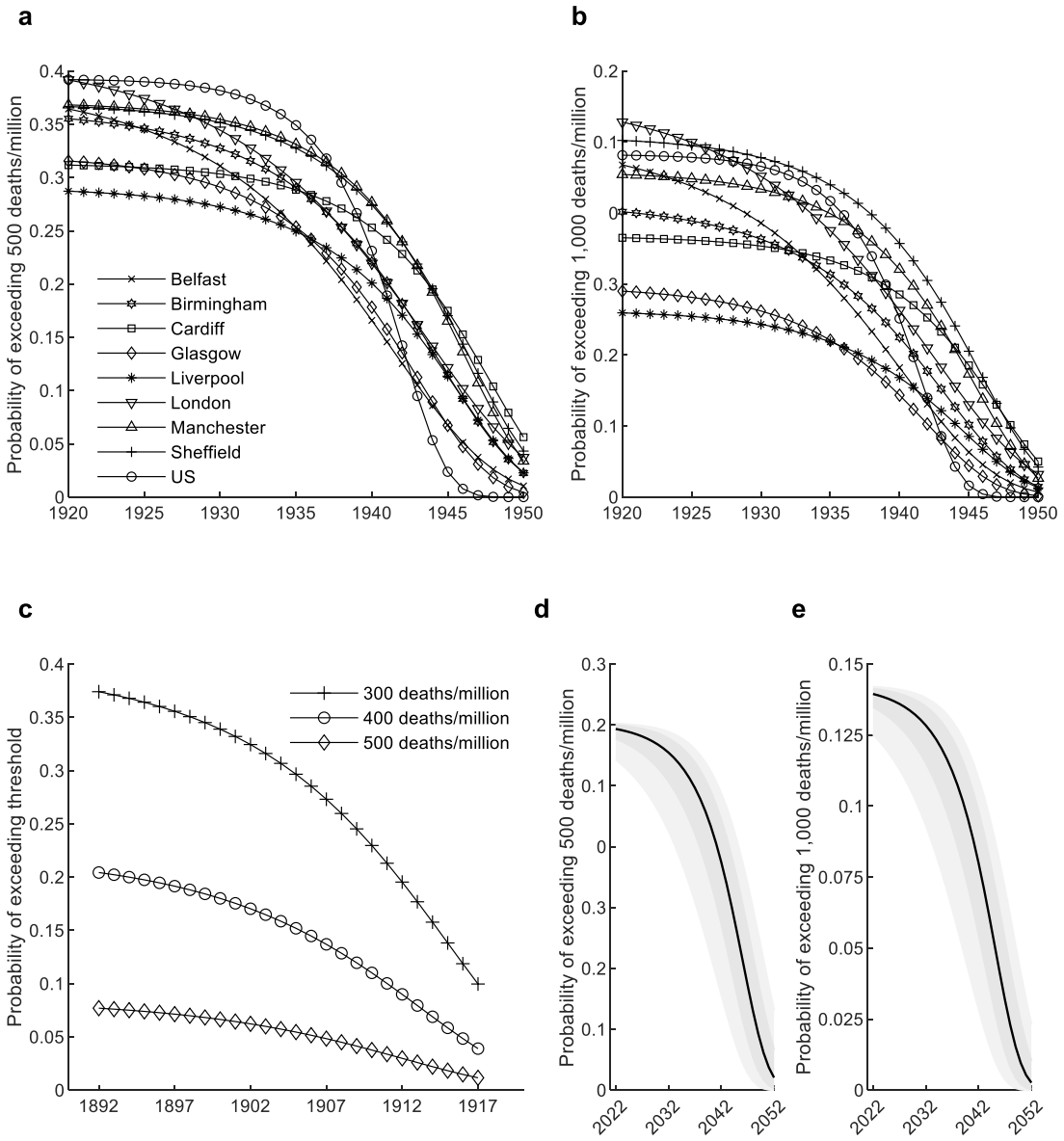


*Figure 3. Outbreak risk following the historical 1918-19 and 1890-91 pandemics and COVID-19. (a)-(b) Outbreak probabilities computed from models fitted to each city and the US, for thresholds of (a) 500 deaths per million and (b) 1000 per million. (c) Outbreak probabilities computed from the model fitted to data for England and Wales following the 1890-91 pandemic, for different thresholds. (d)-(e) Simulated outbreak probabilities for COVID-19, showing median (solid black line), interquartile range (dark shading) and 80% prediction interval (light shading), based on 1m random draws. Outbreak probabilities are computed from model parameterisations that are drawn from a distribution of $\eta_0$ and $\lambda$ implied by the models fitted to historical data. The upper bound on future mortality ($d_u$ = 1858) is set equal to COVID-19 mortality in the UK in 2020 and the lower bound ($d_l$ = 24) to reflect mortality in the non-pandemic state, approximated by background influenza mortality pre-2020 (data sources in SI).*

Figure 3 (d)-(e) shows model-predicted probabilities of disease outbreaks (mortality rates exceeding 500 and 1000 per million) from a counterfactual analysis after the main waves of COVID-19, allowing for model uncertainty.

These results demonstrate elevated disease outbreak risk for two decades. In 90% of model-predicted dynamic paths, the probability of outbreaks exceeding 500 deaths per million, which is 20 times higher than seasonal influenza, is above 20% for a decade and remains above 10% for two decades. Regarding outbreaks closer in scale to mortality during the first main wave, in 90% of model-predicted dynamic paths, the probability of outbreaks exceeding 1000 deaths per million is above 10% for a decade.

**Concluding remarks**

The similarity of the pattern of disease outbreak dynamics across geographic units with different socioeconomic characteristics and two historical pandemics highlights the generality of our finding that mortality risk remains elevated for a prolonged period after the main pandemic waves.

Our findings can inform research to understand the implications of pandemics for a range of health and socioeconomic outcomes by quantifying post-pandemic mortality risk and its persistence over time. Disease outbreak risk generates health and economic uncertainty, which has significant and unequal consequences for socioeconomic outcomes across the population. Given that disease outbreaks imply a deterioration in health outcomes that is not symmetric across the population (e.g. Quinn and Kumar (2014), Marmot (2020), Marmot and Allen (2020) and Mamelund and Dimka (2021)), a period of increased disease outbreak risk implies the possibility of repeated negative shocks to health inequality. Moreover, outbreak risk generates social, political and economic uncertainty, stemming from possible impacts of the disease itself and of containment measures on economic activity. Increased aggregate-level uncertainty further impacts economic decision-making, income inequality and economic fluctuations, either directly or via increased idiosyncratic risk (e.g. Heathcote *et al.* (2010), Bloom (2009), Bloom *et al.* (2018) and Angelopoulos *et al.* (2021a, 2020)).

The potentially high persistence of disease outbreak risk for many years after a pandemic highlights the value of scientific and medical developments. Indeed, medicine, public health, technology, and better-informed and prepared policy intervention offer the opportunity in the modern world to confront post-pandemic recurrent outbreak risk better than a century ago. The overall message from our analysis is that ongoing prevention strategies and policy preparedness to mitigate outbreaks are likely to be required, even well after the main pandemic waves.

## References


Anderson, R.M., May, R.M. (1992). *Infectious Diseases of Humans: Dynamics and Control*, Oxford Science Publications

Angelopoulos, K., Lazarakis, S., Malley, J. (2020). The distributional implications of asymmetric income dynamics, *European Economic Review*, 128, 103502, https://doi.org/10.1016/J.EUROECOREV.2020.103502

Angelopoulos, K., Lazarakis, S., Malley, J. (2021a). Cyclical labour income risk in Great Britain, *Journal of Applied Econometrics*, https://doi.org/10.1002/JAE.2860

Angelopoulos, K., Lazarakis, S., Mancy, R., Schroeder, M. (2021b). Pandemic-induced wealth and health inequality and risk exposure, *CESifo Working Paper*, No. 9474, https://www.cesifo.org/DocDL/cesifo1_wp9474.pdf

Bloom, N. (2009). The Impact of Uncertainty Shocks, *Econometrica* 77, 623–685, https://doi.org/10.3982/ecta6248

Bloom, N., Floetotto, M., Jaimovich, N., Saporta-Eksten, I., Terry, S.J. (2018). Really Uncertain Business Cycles, *Econometrica*, 86, 1031–1065, https://doi.org/10.3982/ecta10927

Cirillo, P., Taleb, N.N. (2020). Tail risk of contagious diseases, *Nature Physics*, 16:6 16, 606–613. https://doi.org/10.1038/s41567-020-0921-x

Giannitsarou, C., Kissler, S., Toxvaerd, F. (2021). Waning immunity and the second wave: Some projections for SARS-CoV-2, *American Economic Review: Insights*, 3, 321–338

Heathcote, J., Storesletten, K., Violante, G.L. (2010). The macroeconomic implications of rising wage inequality in the United States, *Journal of Political Economy*, 118, 681–722, https://doi.org/10.1086/656632

Kissler, S.M., Tedijanto, C., Goldstein, E., Grad, Y.H., Lipsitch, M. (2020). Projecting the transmission dynamics of SARS-CoV-2 through the postpandemic period, *Science*, 368, 860–868, https://doi.org/10.1126/science.abb5793

Lavine, J.S., Bjornstad, O.N., Antia, R. (2021). Immunological characteristics govern the transition of COVID-19 to endemicity, *Science*, 371, 741–745, https://doi.org/10.1126/science.abe6522

Madhav, N., Oppenheim, B., Gallivan, M., Mulembakani, P., Rubin, E., Wolfe, N. (2017). Pandemics: Risks, Impacts, and Mitigation, in: *Disease Control Priorities: Improving Health and Reducing Poverty*, 3rd Edition, The International Bank for Reconstruction and Development/The World Bank

Mamelund, S.-E., Dimka, J. (2021). Social inequalities in infectious diseases, *Scandinavian Journal of Public Health*, 140349482199722, https://doi.org/10.1177/1403494821997228

Marmot, M. (2020). *Health equity in England: The Marmot review 10 years on*, The BMJ 368, m693. https://doi.org/10.1136/bmj.m693

Marmot, M., Allen, J. (2020). COVID-19: exposing and amplifying inequalities, *Journal of Epidemiology and Community Health*, 74, jech-2020-214720, https://doi.org/10.1136/jech-2020-214720

McKie, R. (2021). UK can expect thousands of Covid deaths every year, warn scientists | Coronavirus | The Guardian [WWW Document], the Guardian. URL https://www.theguardian.com/world/2021/jul/31/uk-can-expect-thousands-of-covid-deaths-every-year-warn-scientists?CMP=Share_iOSApp_Other (accessed 8.18.21).

Oxford, J.S. (2000). Influenza A pandemics of the 20th century with special reference to 1918: virology, pathology and epidemiology, R*eviews in medical virology*, 10, 119–133, https://doi.org/10.1002/(SICI)1099-1654(200003/04)10:2

Phillips, N. (2021). The coronavirus is here to stay — here's what that means, *Nature*, 590, 382–384, https://doi.org/10.1038/d41586-021-00396-2

Quinn, S.C., Kumar, S. (2014). Health inequalities and infectious disease epidemics: A challenge for global health security, *Biosecurity and Bioterrorism*, 12, 263–273. https://doi.org/10.1089/bsp.2014.0032

Scheidel, W. (2018). *The great Leveler*, Princeton University Press

Stantcheva, S. (2021). Inequalities in the Times of a Pandemic, *Economic Policy*

Supplementary Information for

# How do pandemics end? Two decades of recurrent outbreak risk following the main waves.

Max Schroeder, Spyridon Lazarakis, Rebecca Mancy, Konstantinos Angelopoulos

**This PDF file includes:**

**Contents**

## A. Data sources

City-level data were compiled from Medical Officer of Health (MOH) reports. These reports were annual administrative documents covering a range of public health-related issues at the municipal level. The first reports begin in the mid-19th century, and coverage extends to most municipalities in the UK until the early 1970s. The reports used here have been digitised and can be viewed on the Wellcome Trust Collection website (Wellcome Trust, 2021).

We collected influenza mortality data between 1895 and 1950 for eight large municipalities from across the UK: Belfast, Birmingham, Cardiff, Glasgow, London, Liverpool, Manchester and Sheffield. To do this, we searched relevant MOH reports for each municipality. Generally, annual mortality rates by cause of death are presented in tables within the report or its appendices (or could be computed as the ratio of the number of deaths to the population size). Despite changes over time to the taxonomy of causes of death, *influenza* was reported in the MOH reports throughout the decades. During the war years, 1914-1919 and 1939-1945, some reports are missing, or the data provided is incomplete. In these cases, we recovered the missing information by assessing statistics for these years from later reports, where possible. The dataset collected from the MOH reports underlying this research paper is available on GitHub at https://github.com/maxschr90/Schroeder-et-al.-2021--How-long-do-pandemics-last-.

The narrative provided in the MOH reports for London County Council confirms that the two decades after the three initial waves of the pandemic were characterised by several further large influenza outbreaks. In particular, we examined available London County Council MOH reports between 1920 and 1957 to identify discussions of increased prevalence of influenza in a given year. In each report, we performed a search for the phrase *influenza*. As public health officials were particularly attentive to influenza after the 1918-19 pandemic, virtually every annual report contains at least some discussion of the disease. Generally, the language of the reports is clear on whether a certain year is considered to have a notable outbreak of influenza. Some reports further included retrospective reflections on past influenza outbreaks. The reports identify 1922, 1924, 1927, 1929, 1933 and 1937 as years of heightened mortality from influenza relative to other years.

Data for the US are taken from the annual vital statistics reports compiled by the National Center for Health Statistics. Specifically, we rely on the two special volumes (Grove and Hetzel (1968) and Linder and Grove (1943)) covering the period 1900-1960. Both volumes are available on the CDC's website. Data for England and Wales between 1838 and 1917 are taken from Langford (2002, Table 5), who compiles mortality rates from different sources.

To obtain COVID-19 mortality for the analysis in Figure 2 (d)-(e), we combined the total number of UK COVID-19 deaths between 6th March 2020 and 6th March 2021 (124,654) (Ritchie et al. 2020). With mid-year population data from the ONS for 2020 (67,081,000) (ONS, 2021a). This implies a mortality rate of 1,858 per million. Pre-2020 deaths from influenza are taken from the 2018-19 total mortality figures for England & Wales from the ONS (ONS, 2021b) together with the mid-2018 population figures for England & Wales (ONS, 2019).

| | Population | | | Population density | | |
|---|---|---|---|---|---|---|
| | 1920s | 1930s | 1940s | 1920s | 1930s | 1940s |
| Belfast | 422,130 | 425,202 | 442,935 | - | - | - |
| Birmingham | 947,923 | 1,023,811 | 1,053,157 | 5,185 | 4,938 | 5,185 |
| Cardiff | 219,894 | 222,658 | 227,861 | 5,185 | 4,444 | 1,728 |
| Glasgow | 1,079,858 | 1,088,829 | 1,089,368 | 12,593 | 8,642 | 6,667 |
| Liverpool | 837,595 | 858,783 | 720,112 | 9,877 | 7,901 | - |
| London | 4,540,000 | 4,230,295 | 2,863,548 | - | - | - |
| Manchester | 749,970 | 746,974 | 641,040 | 8,642 | 7,160 | 5,926 |
| Sheffield | 519,224 | 517,967 | 492,093 | 1,728 | 3,457 | 3,210 |

*Table A-1: Population and density for UK cities. Population and population density numbers refer to decadal averages compiled from available data in the MOH reports. Population density is measured in persons/km².*

## B. Details of model of mortality risk dynamics

### *Details of baseline model*

The model in (1) – (2) assumes that mortality rates after the main waves of the pandemic are the outcomes of a sequence of bounded Pareto distributions, where the inverse of the tail index of these distributions decays exponentially over time. The parameters $d_l > 0$ and $d_u > d_l$ scale the range of mortality rates that the model predicts. We fit the model to the data for each geographical unit and conditional on its experience of the pandemic. Hence, we choose the bounds to reflect the realised range of mortality rates for the geographical unit over the period modelled. Conditional on $d_l$ and $d_u$, the two parameters $\eta_0$ and $\lambda$ then determine the dynamics of mortality and disease outbreak risk via controlling the level and time evolution of probabilities of outcomes associated with the tail of the Pareto distributions.

We obtain $\lambda$ and $\eta_0$ by maximising the likelihood function:

$$L(\lambda, \eta_0) = \prod_{t=0}^{N} \frac{\left(\eta_0 e^{-\lambda t}\right)^{-1} (d_l)^{\left(\eta_0 e^{-\lambda t}\right)^{-1}} (\bar{d}_t)^{-\left(\eta_0 e^{-\lambda t}\right)^{-1}-1}}{1-\left(\frac{d_l}{d_u}\right)^{\left(\eta_0 e^{-\lambda t}\right)^{-1}}}, \qquad (3)$$

given a sample of mortality rates $\left(\bar{d}_t\right)_{t=0}^{N}$. To maximise the log likelihood function, we use MATLAB's fmincon routine, using a sequential quadratic programming algorithm. Derivatives are approximated by central numerical derivatives, and the relevant termination criteria are set to $1e^{-12}$. To account for potential nonconvexities and the presence of local maxima, we begin the maximisation from 1000 random seed values. Parameters are provided in table B-1 below:

| | $\lambda$ | $\eta_0$ | $d_l$ | $d_u$ |
|---|---|---|---|---|
| **City average** | 0.151 | 76.867 | 24 | 3059 |
| | (0.030) | (48.638) | | |
| Belfast | 0.119 | 24.859 | 22 | 3644 |
| | (0.025) | (14.042) | | |
| Birmingham | 0.144 | 58.442 | 30 | 2497 |
| | (0.034) | (47.222) | | |
| Cardiff | 0.184 | 360.214 | 13 | 2671 |
| | (5.094) | (491.962) | | |
| Glasgow | 0.166 | 74.119 | 33 | 1812 |
| | (0.033) | (57.663) | | |
| Liverpool | 0.166 | 126.778 | 23 | 1775 |
| | (0.031) | (83.284) | | |
| London | 0.11 | 26.352 | 23 | 4458 |
| | (0.025) | (12.899) | | |
| Manchester | 0.18 | 208.861 | 23 | 3067 |
| | (0.034) | (160.107) | | |
| Sheffield | 0.169 | 202.69 | 12 | 4550 |
| | (0.033) | (143.300) | | |
| **US** | 0.278 | 802.709 | 31 | 3018 |
| | (0.034) | (642.435) | | |
| **England & Wales** | 0.111 | 7.684 | 113 | 574 |
| | (0.057) | (8.956) | | |

*Table B-1: Model parameters. Maximum likelihood estimates of the baseline model specification described in the main text. Numerical standard errors in parentheses.*

***Model with common mortality bounds***

The choice of the bounds, $d_l$ and $d_u$, scales the range of mortality rates. In the baseline application, $d_u$ for each city is set to the mortality rate of 1918 for that city, and $d_l$ to lowest mortality experienced in the long run in each city, or the average across cities for the model fitted to the average. For the US following the 1918-19 pandemic, $d_l$ and $d_u$ are the lowest post-1918 and the 1918 mortality rates observed in the US time series; for the 1890-91 post-pandemic mortality rate dynamics, these parameters refer to the lowest between 1891 and 1917, and the 1891 mortality rates in the respective time series for England and Wales. These parameters are provided in table B-1.

The advantage of letting $d_l$ and $d_u$ be specific to the geographical unit studied is that we allow for differences in the experience of the pandemic and in conditions that influence background infectious disease mortality to have a bearing on risk dynamics. By allowing for such latent variation, our finding of a general pattern of mortality and disease outbreak risk dynamics is stronger. Indeed, if we set $d_l$ and $d_u$ to be common across all cities, specifically to the lowest and highest mortality rate observed across them, the overall pattern is very similar across cities; that is, compared with the results in Figure 3 (a-b), even greater similarity is observed. In contrast, the results in Figure 3 (a-b) reassure us that the general pattern remains similar even after controlling for variation between cities. The results from setting common bounds are shown in figure B-1 below. This agnostic modelling of $d_l$ and $d_u$ confirms high and persistent mortality risk after the main pandemic waves, as well as similarity across geographical units, but, compared with the post-pandemic experience, it exaggerates it relative to actual experience. On the other hand, exploiting the information pertinent to the pandemic in parameterising $d_l$ and $d_u$ leads to more accurate mortality risk predictions.

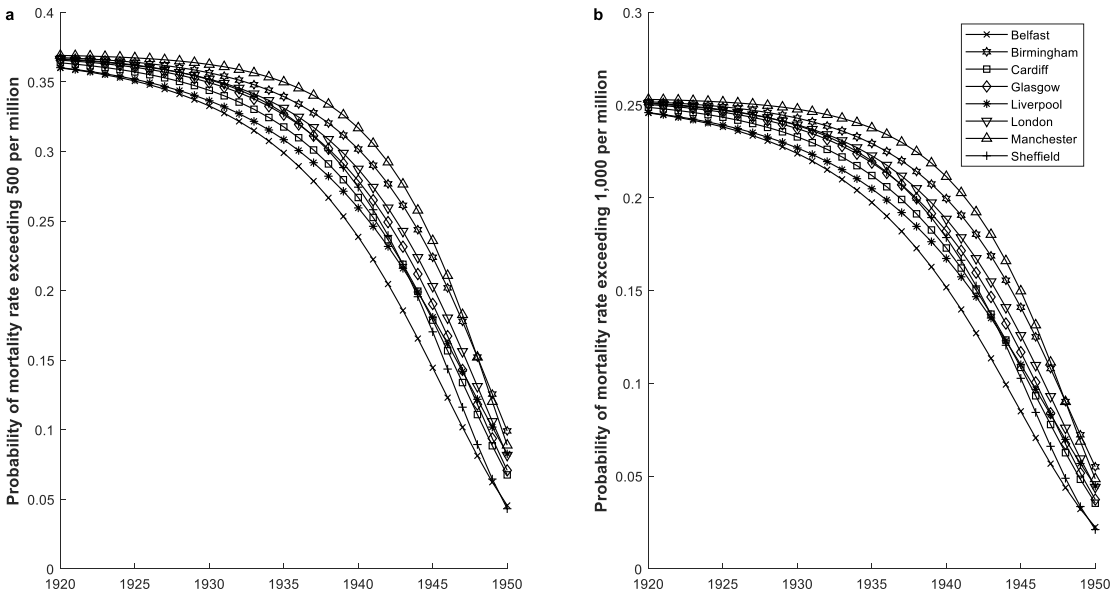


*Figure B-1: Outbreak risk following the 1918-19 pandemic (model with common bounds). Outbreak probabilities computed from models fitted to each city. Upper and lower bounds are common and set to be the highest and lowest mortality rates within the sample of cities respectively.*

### *Model with theoretical mortality bounds*

We next compare the approach of specifying the bounds of the Pareto distribution conditionally on the mortality range relevant to the geographical unit to a more agnostic approach of setting $d_u$ and $d_l$ to be determined theoretical upper and lower bounds of mortality rates. Figure B-2 reproduces Figures 3 (a-b) under the agnostic modelling approach. As can be seen, in Figure B-3 the probability of a disease outbreak remains high until the 1940s, the dynamic pattern is different from that in Figure 3 (a-b), implying disease outbreak risk that is very high initially and declines more rapidly. Overall, agnostic modelling of $d_l$ and $d_u$ confirms high and persistent mortality risk after the main pandemic waves, as well as similarity across geographical units, but, compared with the post-pandemic experience, it exaggerates it relative to the actual experience. On the other hand, exploiting the information pertinent to the pandemic in parameterising $d_l$ and $d_u$ leads to more accurate mortality risk predictions.

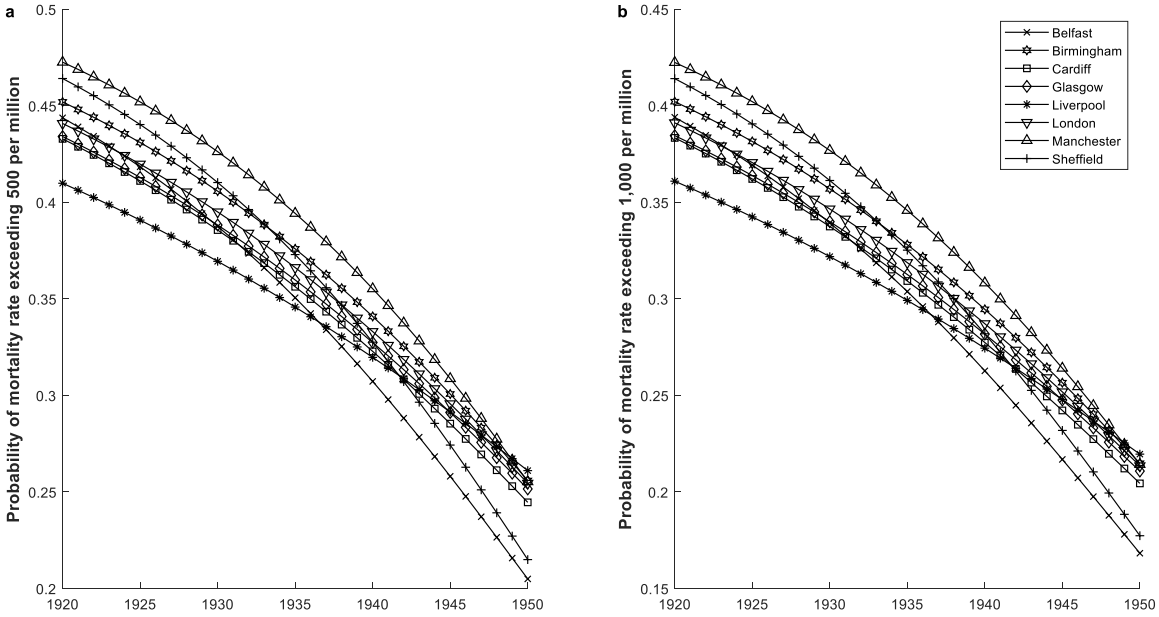


*Figure B-2: Outbreak risk following the 1918-19 pandemic (model with theoretical bounds). Outbreak probabilities computed from models fitted to each city. Upper and lower bounds are set to 1,000,000 and 1 respectively.*

***Model with estimated mortality bounds***

Technically, $d_l$ and $d_u$ can be estimated jointly with $\eta_0$ and $\lambda$ using the time series following the main pandemic waves (i.e., without exploiting the information on the mortality effect of the main pandemic waves). In this case, (3) is maximised by choosing all four parameters, following the same optimisation methods as for the model in (1) – (2). Figures B-3 and B-4 reproduce Figures 2 and 3 (a-b) under this methodology.

However, the model predictions in this case do not capture disease outbreak risk. In particular, although fitting the model in (1) – (2) by estimating all four parameters from the time series of data following the main pandemic waves may be useful for some applications (e.g. if the interest is in summarising historical experience), conceptually, this is no longer a model of mortality and disease outbreak *risk* dynamics, i.e. of the time evolution of the probability of disease outbreaks. Instead, $d_l$ and $d_u$ should be interpreted as parameters chosen to maximise the fit of the process to the data, and thus are chosen by the optimisation routine to be in effect the maximum and minimum mortality observed between 1920 and 1950. In turn, this rules out the possibility of disease outbreaks that are higher than those observed *ex post*, even if theoretically they could have happened. An analysis of risk dynamics must account for the possibility of higher mortality than that that was actually observed. Our modelling approach views bounds as *possible* even if unrealised mortality rates, given the experience of the pandemic, which determines the upper bound, and given the expectation about background mortality that is unaffected by the pandemic, which determines the lower bound. Indeed, if we simply fit the model to the post-pandemic data by estimating $d_l$ and $d_u$ jointly with $\eta_0$ and $\lambda$ using the time series following the main pandemic waves, we find that the model predicted mortality is close to the actual path of mortality, while disease outbreak probabilities for large outbreaks are reduced.

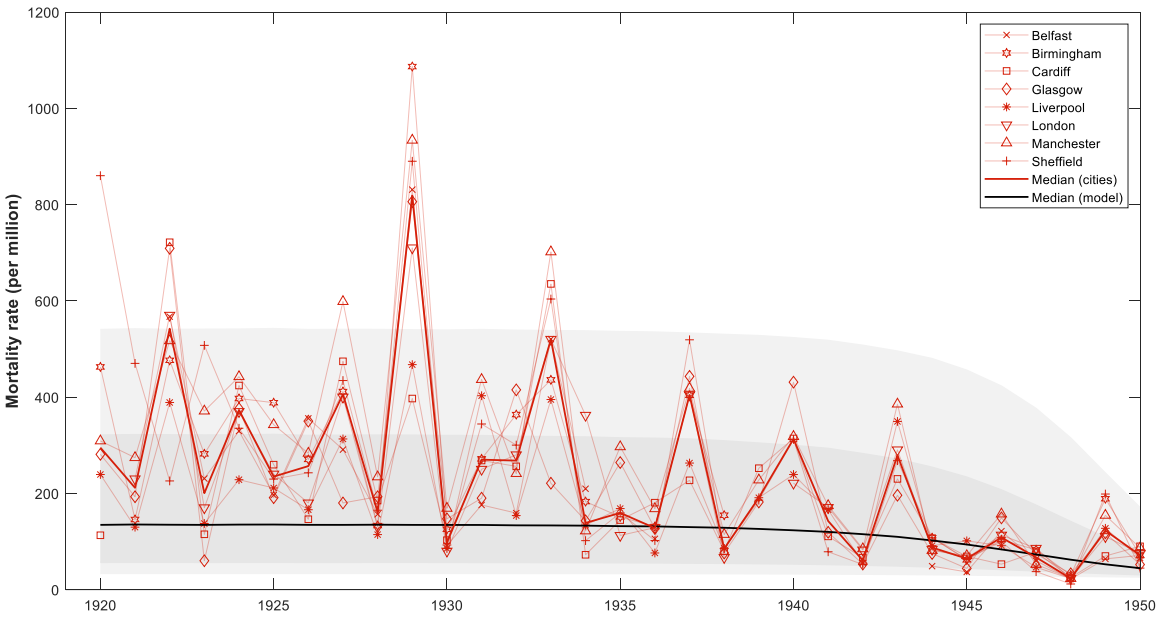


*Figure B-3: Model predicted influenza mortality rates following the 1918-19 pandemic (model with estimated bounds). Simulated median (solid black line), interquartile range (dark shading) and 80% prediction interval (light shading) are based on 1m random draws. Simulated outcomes are based on the model fitted using the average across cities. Upper and lower bounds are fitted to the data. Data are overplotted in red. Data for UK cities are taken from Medical Officer for Health reports.*

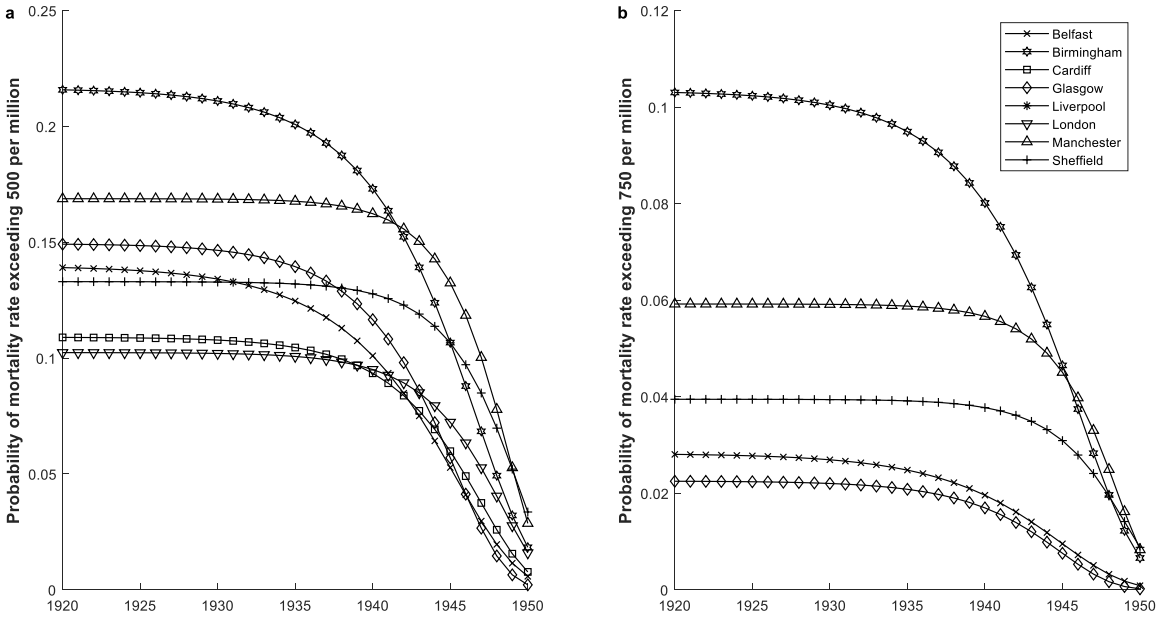


*Figure B-4: Outbreak risk following the 1918-19 pandemic (model with estimated bounds). Outbreak probabilities computed from models fitted to each city. Upper and lower bounds are fitted to the data (1920-1950) for each city.*

***One-parameter Weibull model***

To further illustrate key points of the relevance of the Pareto distribution, we describe and fit a model with an alternative one-parameter distribution that allows for high probabilities for outcomes associated with the tail, the one-parameter Weibull-type distribution (Alexopoulos (2019)). In this case, mortality rates are drawn from:

$$d_t \sim W_t(w_t), \quad (4)$$

where $w_t \in [0,1]$, noting that the tail contracts as $w_t$ decreases. Assume that:

$$w_t = w_0 e^{-\lambda t}. \quad (5)$$

Conditional on the time process in (5), and thus conditional on the sequence $(w_t)_{t=0}^{N}$, $d_t$ is independently distributed over time following (4). The likelihood is given by:

$$L(\lambda, w_0) = \prod_{t=0}^{N} \frac{log^3(w_0 e^{-\lambda t})}{log(w_0 e^{-\lambda t})-2} \bar{d}_t \left(\bar{d}_t + 1\right)\left(w_0 e^{-\lambda t}\right)^{\bar{d}_t},$$

for a sample of mortality rates $\left(\bar{d}_t\right)_{t=0}^{N}$. The results from this model, shown in figures B-5 and B-6 also reveal that mortality risk remains high for a long period after the main pandemic waves, and that its dynamic pattern is similar across geographical units. However, the predicted probabilities for disease outbreaks are higher than those in Figure 3 (a-b). This is an implication of the one-parameter Weibull form that delivers a fat tail by shifting the mass of the distribution away from lower numbers (Alexopoulos, 2019). Moreover, disease outbreak risk inherits a rate of rapid decline from the exponential decay of $w_t$, the Weibull parameter that determines the thickness of the tail. This analysis demonstrates the importance of the property of the Pareto distribution that it can accommodate a fat tail with the mass of the distribution near the lower bound of outcomes. Alternative distributions that can deliver a concentration at lower mortality levels while also allowing for high probabilities associated with tail outcomes require more parameters to be specified (e.g. lognormal, Gaussian mixture) and require more assumptions regarding the dynamic transition. In particular, the model must specify the dynamic evolution of two or more parameters and a means to identify the specific combination of the dynamic processes of these parameters that characterises the evolution of tail probabilities and of mortality risk more generally. Data availability restricts these options. Being a one-parameter distribution conditional on the bounds for mortality rates, the bounded Pareto offers a transparent way to model the post-pandemic dynamic evolution of mortality and disease outbreak risk.

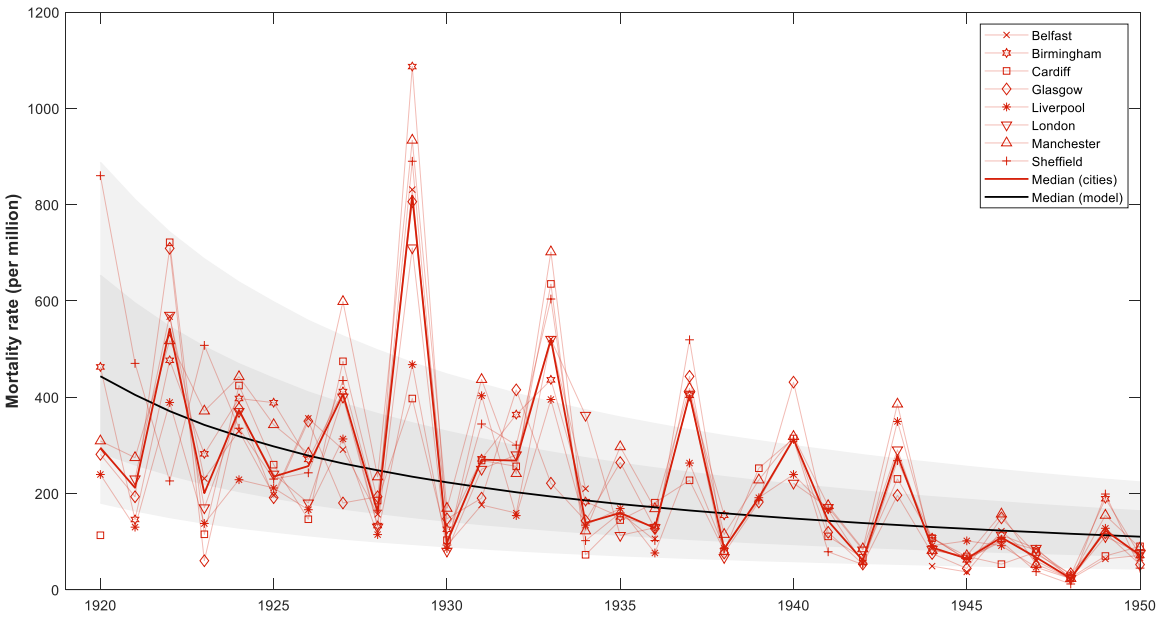


*Figure B-5: Model predicted influenza mortality rates following the 1918-19 pandemic (One-parameter Weibull model). Simulated median (solid black line), interquartile range (dark shading) and 80% prediction interval (light shading) are based on 1m random draws. Simulated outcomes are based on the model assuming a sequence of one-parameter Weibull distributions fitted using the average across cities (1920-1950). Data are overplotted in red. Data for UK cities are taken from Medical Officer for Health reports.*

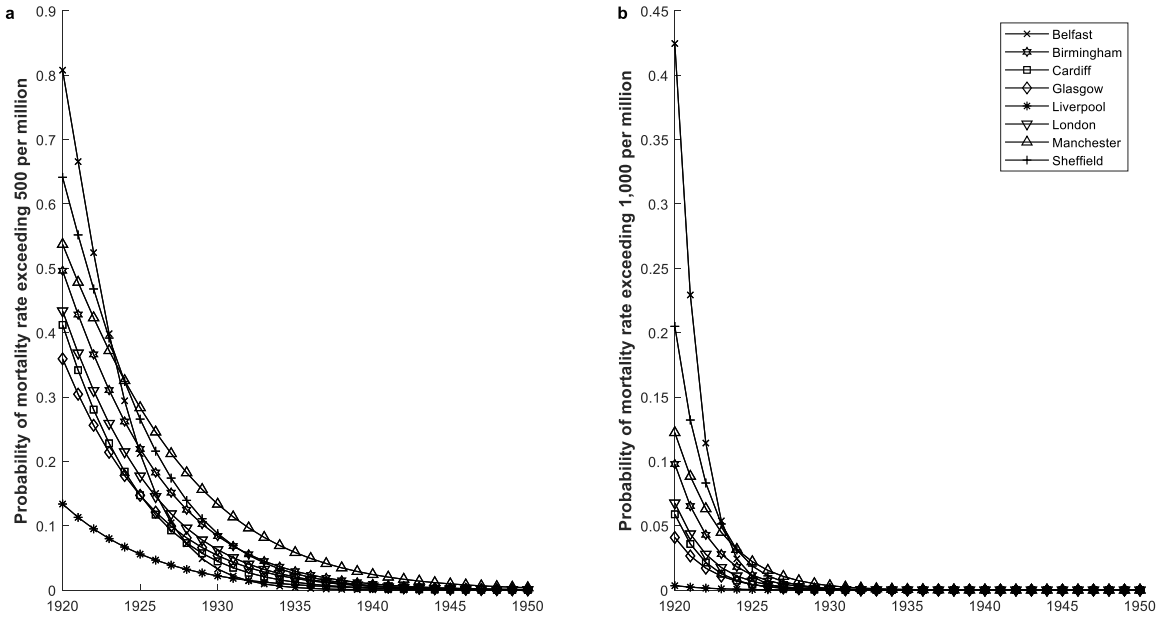


*Figure B-6: Outbreak risk following the 1918-19 pandemic (One-parameter Weibull model). Outbreak probabilities computed from models fitted to each city assuming a sequence of one-parameter Weibull distributions.*

***Details of modelling uncertainty***

To account for model uncertainty, we assume that the parameters $\eta_0$ and $\lambda$ that are relevant to a new pandemic are drawn from the same distribution from which the parameters in table B-1 are drawn, and then perform a Monte Carlo analysis that provides a distribution of possible outcomes as a function of draws of $\eta_0$ and $\lambda$ from that distribution. Using the parameter values of $\eta_0$ and $\lambda$ in table B-1, we estimate the underlying distribution and approximate it as a joint lognormal:

$$\begin{pmatrix}\log(\eta_0)\\ \log(\lambda)\end{pmatrix} \sim MVN(\mu, \sigma)$$

$$\mu = \begin{pmatrix}-1.85\\ 4.5\end{pmatrix}, \sigma = \begin{pmatrix}0.08 & 0.37\\ 0.37 & 1.96\end{pmatrix}$$

We then draw one million pairs of $\eta_0$ and $\lambda$ from the implied joint density and summarise relevant percentiles of the generated distribution of predicted probabilities of mortality rates in Figure 3 (d-e).

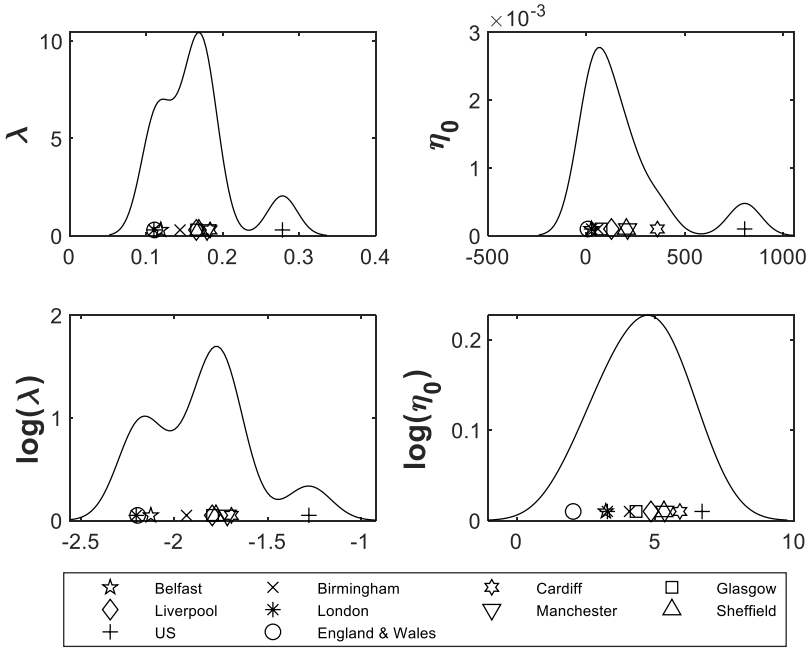


*Figure B-7: Distribution of $\eta_0$ and $\lambda$ implied by the models fitted to previous pandemics. Kernel density estimates.*

## C. Additional Figures

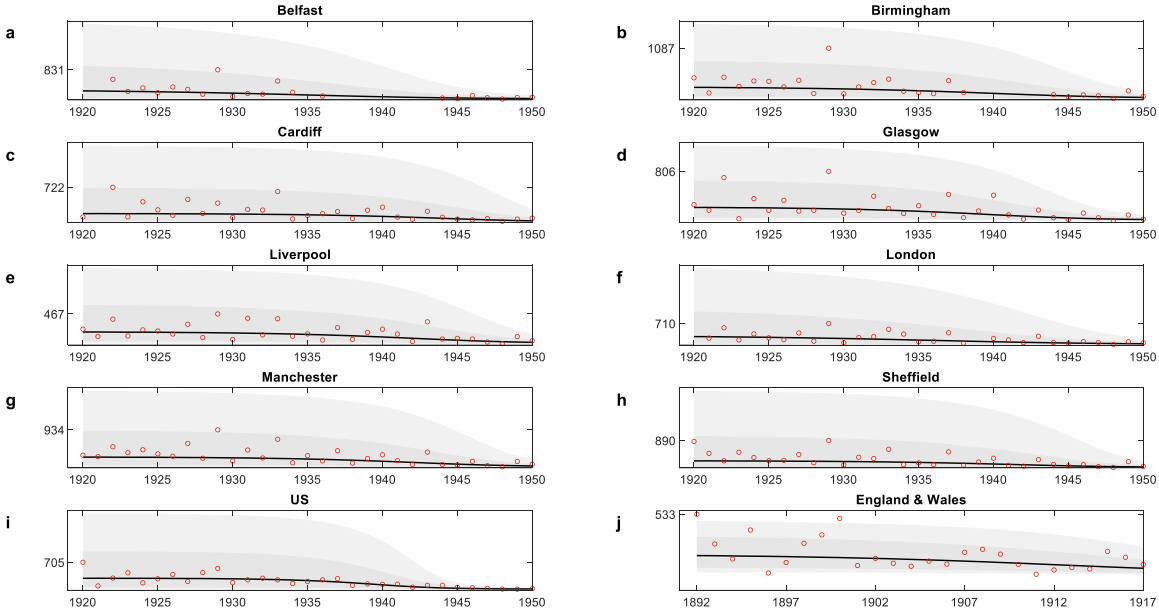


*Figure C-1: Model predicted influenza mortality rates following the 1918-19 and 1890-91 pandemics (deaths per million). Simulated median (solid black line), interquartile range (dark shading) and 80% prediction interval (light shading) are based on 1m random draws. Simulated outcomes are based on the model fitted to each city, the US and England & Wales. Data for UK cities are taken from Medical Officer for Health reports. Data for the US is taken from Lindner and Grove (1943) and Grove and Hetzel (1968). Data for England & Wales are taken from Langford (2002), Table 5.*

## D. References


Alexopoulos, A. (2019). One-Parameter Weibull-Type Distribution, Its Relative Entropy with Respect to Weibull and a Fractional Two-Parameter Exponential Distribution, *Stats*, 2, 34–54. https://doi.org/10.3390/stats2010004

Grove, R.D., Hetzel, A.M. (1968). *Vital statistics rates in the United States, 1940-1960*, US Department of Health, Education, and Welfare, Public Health Service

Langford, C. (2002). The age pattern of mortality in the 1918-19 influenza pandemic: an attempted explanation based on data for England and Wales, *Medical History*, 46, 1–20. https://doi.org/10.1017/S002572730006871X

Linder, F.E., Grove, R.D. (1943). *Vital statistics rates in the United States, 1900-1940*, US Government Printing Office

ONS (2021a). Population estimates - Office for National Statistics [WWW Document], URL https://www.ons.gov.uk/peoplepopulationandcommunity/populationandmigration/populationestimates (accessed 8.18.21)

ONS (2021b). Influenza deaths in 2018, 2019 and 2020 - Office for National Statistics [WWW Document], URL https://www.ons.gov.uk/aboutus/transparencyandgovernance/freedomofinformationfoi/influenzadeathsin20182019and2020 (accessed 8.18.21)

ONS (2019). Population estimates for the UK, England and Wales, Scotland and Northern Ireland - Office for National Statistics [WWW Document], URL https://www.ons.gov.uk/peoplepopulationandcommunity/populationandmigration/populationestimates/bulletins/annualmidyearpopulationestimates/mid2018 (accessed 8.18.21)

Ritchie, H., Ortiz-Ospina, E., Beltekian, D., Mathieu, E., Hasell, J., Macdonald, B., Giattino, C., Appel, C., Rodés-Guirao, L., Roser, M. (2020). Coronavirus Pandemic (COVID-19) [WWW Document]. Published online at OurWorldInData.org. URL https://ourworldindata.org/coronavirus/country/united-kingdom#what-is-the-cumulative-number-of-confirmed-deaths (accessed 8.18.21)

Wellcome Trust (2021). The Medical Officer of Health reports [WWW Document]. URL https://wellcomelibrary.org/moh/about-the-reports/about-the-medical-officer-of-health-reports/ (accessed 8.18.21)

**Acknowledgements and funding**
We would like to thank Irene O'Brien at Glasgow City Archives for guidance on archival data, Rosie Sida for help with data preparation, and Dan Haydon, Sema Nickbakhsh, Richard Reeve and Denise Brown for comments on an earlier version of this work.

This project is supported by a grant that is funded by the Economic and Social Research Council (ESRC) as part of UK Research and Innovation's rapid response to COVID-19 (ES/V005898/1). The project also received support from the College of Social Sciences College Research Fund 2020/21, and from the Adam Smith Business School Student Internship Scheme, University of Glasgow. The project is supported by Glasgow City Archives, Glasgow Life. Rebecca Mancy is supported by The Leckie Fellowship, the UK Medical Research Council (MRC) Places and Health Programme (MC_UU_00022/4) and the Chief Scientist Office (CSO) (SPHSU10) at the MRC/CSO Social and Public Health Sciences Unit, University of Glasgow.

**Other versions**
Schroeder, M., Lazarakis, S., Mancy, R., Angelopoulos, K. (2021). How do pandemics end? Two decades of recurrent outbreak risk following the main waves [preprint]. https://doi.org/10.21203/rs.3.rs-893004/v2

**Data availability**
The municipal level dataset generated during the current study are available on GitHub at https://github.com/maxschr90/Schroeder-et-al.-2021--How-long-do-pandemics-last-. Data for the US and for England and Wales are available from original publications, as described and referenced in the caption of Figure 1.

**Code availability**
Code is available on GitHub at https://github.com/maxschr90/Schroeder-et-al.-2021--How-long-do-pandemics-last-.